Pergamon

0042-6989(94)00206-1

Vision Res. Vol. 35, No. 11, pp. 1595–1609, 1995

0042-6989/95 $9.50 + 0.00

Adaptation Mechanisms in Spatial Vision—II. Flash Thresholds and Background Adaptation

PHILIP T. KORTUM,* WILSON S. GEISLER*†

Received 21 April 1994; in revised form 8 August 1994

To examine how the mechanisms of light adaptation affect spatial pattern vision, contrast detection thresholds were measured for sinusoidal (increment-Gabor) probes on flashed backgrounds in the presence of steady adapting backgrounds. The thresholds for all spatial frequencies (1–12 c/deg), flashed-background intensities (dark to 4 log td) and adapting-background intensities (dark to 4 log td) were adequately described by a simple model consisting of a compressive nonlinearity (a modified Naka–Rushton function), a subtractive adaptation factor, and a multiplicative adaptation factor. For all five subjects the compressive nonlinearity was found to vary systematically with spatial frequency; for all but one subject, the subtractive and multiplicative factors were found to be relatively constant.

Light adaptation Spatial-frequency channels Flash thresholds Multiplicative adaptation Subtractive adaptation

INTRODUCTION

One of the remarkable properties of the visual system is its ability to maintain high sensitivity to small contrasts (as produced, for example, by small differences in surface reflectance) over the enormous range of ambient light levels that occurs in the normal environment. This feat is all the more remarkable given the relatively limited dynamic range and high levels of noise exhibited by single neurons. To maintain sensitivity to small contrasts, the response gain of visual neurons must be kept at a high level; but, because of the limited dynamic range of neurons, the visual system is left vulnerable to the negative effects of response saturation (i.e. loss of contrast resolution). The visual system's solution to this "dynamic-range problem" is three-fold: (i) use separate populations of receptors (rods and cones) to detect contrasts in the lower and upper ranges of ambient intensity; (ii) adjust the retinal illumination level via the pupil reflex; and (iii) adjust the sensitivities of individual visual neurons (for a review see, e.g. Shapley & Enroth-Cugell, 1984; Hood & Finkelstein, 1986; Walraven, Enroth-Cugell, Hood, MacLeod & Schnapf, 1990). All three components contribute to the solution, but the third (iii) is the most significant and is accomplished within the photoreceptors and other visual neurons through neural and photochemical adaptation.

Psychophysical and physiological studies indicate two major classes of adaptation mechanisms. One class is multiplicative—adaptation mechanisms equivalent to multiplying input intensities by a variable factor between 0 and 1 (a gain factor). The other class is subtractive—adaptation mechanisms equivalent to subtracting a variable factor from the input intensities. The ability of the human visual system to detect spatial patterns is controlled by these adaptation mechanisms, and by other factors, including the response nonlinearities and spatial-frequency selectivities of visual neurons.

The previous paper in this series (Hahn & Geisler, 1995) reported detection thresholds for sine-wave grating targets (probes); measurements were made during dark adaptation following full bleaches, and on steady backgrounds of various intensities. The results indicated a fundamental difference between bleaching and background adaptation. Specifically, the shape of the amplitude sensitivity function (amplitude sensitivity plotted as a function of spatial frequency) is constant during dark adaptation, but the shape changes considerably as steady background intensity is increased. The dark adaptation results are consistent with the hypothesis that bleaching adaptation is local and multiplicative, and that it does not otherwise affect the spatial processing properties of the visual system. The results for steady backgrounds indicate that background adaptation is more complicated; it does (in effect) change the spatial processing properties of the visual system.

The purpose of the present study was to systematically examine the effects of background adaptation on spatial pattern detection by measuring amplitude threshold functions on flashed backgrounds as a function of steady background intensity and target spatial frequency.

*Center for Vision and Image Sciences, University of Texas at Austin, Mezes Hall 330, Austin, TX 78712, U.S.A.
†To whom all correspondence should be addressed.

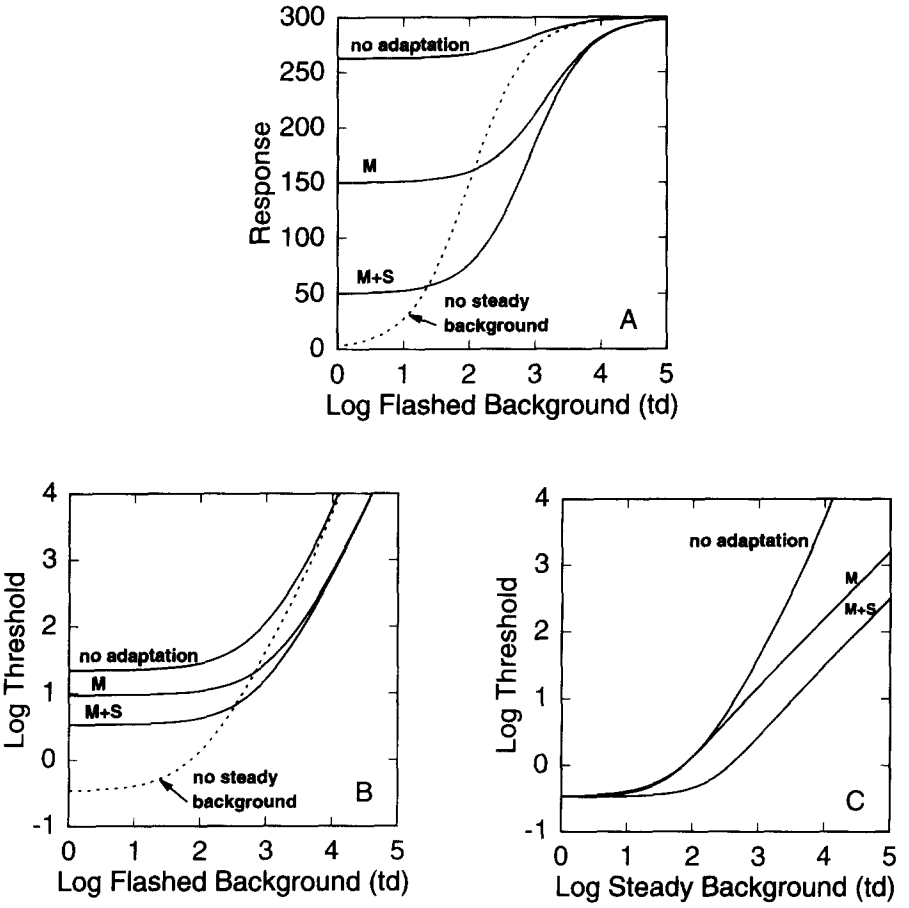

FIGURE 1. Effect of multiplicative and subtractive adaptation on intensity–response functions and increment–threshold functions. (A) Intensity–response functions to brief flashes, $n = 1.0$, $\alpha = 100$, $R_{max} = 300$ [see equation (2)]. The dotted curve is the intensity–response function in the dark-adapted eye, $m = 1.0$, $s = 0.0$. The solid curves are intensity–response functions that would be obtained in the presence of a steady background at 700 td: curve labeled "no adaptation"—no adaptation mechanisms, $m = 1.0$, $s = 0.0$; curve labeled M—multiplicative adaptation alone, $m = 0.143$, $s = 0.0$; curve labeled M + S—multiplicative and subtractive adaptation, $m = 0.143$, $s = 140$. (B) Flashed-background increment-threshold functions (probe–flash curves) corresponding to the intensity–response functions in (A), $\delta = 1$ [see equations (2) and (3)]. The dotted curve is the probe–flash curve for the dark-adapted eye. The solid curves are the probe–flash curves that would be obtained in the presence of a steady background at 700 td: curve labeled "no adaptation"—no adaptation mechanisms; curve labeled M—multiplicative adaptation alone; curve labeled M + S—multiplicative and subtractive adaptation. (C) Steady-background increment–threshold functions (background-adaptation curves). The curve labeled "no adaptation" shows the background-adaptation curve that would be obtained if there were no adaptation mechanisms (it is identical to the probe–flash curve measured in the dark-adapted eye). The curve labeled M shows the background-adaptation curve that would be obtained if only multiplicative adaptation mechanisms were present. The curve labeled M + S shows the background-adaptation curve that would be obtained if both multiplicative and subtractive adaptation were present.

Flashed backgrounds

Much of the physiological evidence concerning the nature of the neural and photochemical adaptation mechanisms has been obtained by measuring intensity–response functions to flashes of light presented under varying adaptation conditions. Intensity–response functions of visual neurons to brief flashes in the dark-adapted eye have a sigmoidal shape when plotted on a log flash intensity axis [see the dotted curve labeled "no steady background" in Fig. 1(A)], and are often described by a generalized Naka–Rushton equation (Naka & Rushton, 1966),

$$R(I) = \frac{R_{max} I^n}{I^n + \alpha^n} \quad (1)$$

where I is the flash intensity, R_{max} is the maximum response, α is the half-saturation constant, and n is an exponent that is typically in the range 0.7–1.0 (e.g. Boynton & Whitten, 1970).*

All vertebrate cones (Kleinschmidt & Dowling, 1975; Normann & Werblin, 1974), including primate cones (Schnapf, Nunn, Meister & Baylor, 1990; Valeton & van Norren, 1982), exhibit some form of multiplicative adaptation—an adaptation which is roughly equivalent to scaling the input intensity by a multiplicative factor, m. Multiplicative adaptation is also seen in other visual neurons (Jacobs, 1965; Sakmann & Creutzfeldt, 1969;

*Another similar descriptive equation which sometimes provides a slightly better fit is given by

$$R(I) = R_{max}\left(1 - 2^{-I^n/\alpha^n}\right).$$

For the present discussion the choice of equation is not crucial.

Virsu & Lee, 1983) and in psychophysical studies (see, for example, Hood & Finkelstein, 1986; Walraven *et al.*, 1990). Multiplicative adaptation has the effect of shifting the intensity–response function to the right on a log intensity axis. In terms of equation (1) this is represented by multiplying the input intensity (in both the numerator and denominator) by a factor m, where $0 < m < 1$. (Note that increasing the half-saturation constant, α, by the scaling factor $1/m$ is an equivalent operation.)

Figure 1(A) illustrates the effect of multiplicative adaptation on an intensity–response function measured against a steady background (e.g. an ambient intensity level). The curve labeled "no adaptation" shows the intensity–response function that would be obtained in the absence of any adaptation mechanisms. As can be seen, the steady background produces a large base response, and hence greatly compresses the range of responses produced by the flashed background. The curve labeled M shows the effect of multiplicative adaptation (i.e. the effect of decreasing m); the base response to the steady background is reduced and the intensity–response function is shifted to the right.

There is also some evidence in vertebrate cones for a subtractive adaptation mechanism (Schnapf *et al.*, 1990)—an adaptation which is roughly equivalent to subtracting a factor, s, from the input—although the psychophysical evidence is more extensive (Geisler, 1981; Hayhoe, Benimoff & Hood, 1987; Hayhoe, Levin & Koshel, 1992; Hood & Finkelstein, 1986; Walraven *et al.*, 1990). The curve M + S in Fig. 1(A) shows the effect of multiplicative adaptation plus subtractive adaptation, where the subtractive adaptation follows the multiplicative adaptation but is prior to the compressive nonlinearity (see Fig. 2). As can be seen in Fig. 1(A), the effect of the subtractive adaptation is to partially cancel the steady background, and hence lower the base response produced by the steady background.

The effects of multiplicative and subtractive adaptation, operating prior to the response nonlinearity, are represented by the following modification of equation (1):

$$R(I) = \frac{R_{\max}[m(I-s)]^n}{[m(I-s)]^n + \alpha^n} \qquad (2)$$

where m is the multiplicative adaptation factor and s is the subtractive adaptation factor. In this equation, I represents the total input intensity, which is the sum of the flashed-background intensity, I_f, and the steady (adapting) background intensity, I_b (i.e. $I = I_f + I_b$). The two adaptation factors, m and s, are both dependent on the adapting background intensity (I_b), but independent of flash intensity (I_f); m can vary from 1 (no adaptation) to 0, and s can vary from 0 (no adaptation) to I_b.

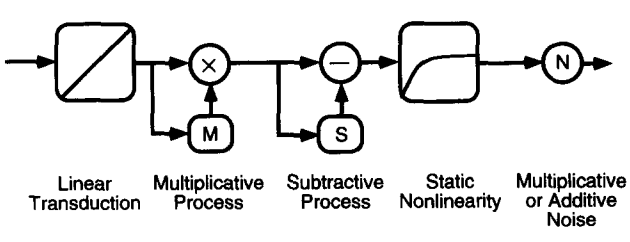

FIGURE 2. A schematic representation of the components of the model described in the text. Following linear transduction, the signal is attenuated by multiplicative adaptation, followed by subtractive adaptation. The signal then passes through a static nonlinearity. Finally, either additive or multiplicative noise is combined with the signal (depending upon the version of the model being tested). It is possible that one or more of these stages varies with target spatial frequency, i.e. that there are multiple channels (although only one channel is shown here).

Evidence of compressive response nonlinearities, multiplicative adaptation mechanisms, and subtractive adaptation mechanisms has been obtained in a variety of psychophysical paradigms (Craik, 1940; Von Kries, 1970; Alpern, Rushton & Torii, 1970; Shevell, 1977, 1978). One of the most informative paradigms involves measuring probe–flash curves (increment–threshold functions for flashed backgrounds) under different fixed adaptation conditions (Hood, Ilves, Mauer, Wandell & Buckingham, 1978; Geisler, 1978, 1981; Hood, 1978; Hayhoe *et al.*, 1987).

The shape of a typical probe–flash curve measured in the dark-adapted fovea (no steady background) is illustrated by the dotted curve in Fig. 1(B). As can be seen, the slope of the curve increases continuously, reaching a value of 2 or more at the highest flashed-background intensities. Such probe–flash curves are accurately predicted by a simple model consisting of an intensity–response function in the form of equation (2), together with the assumption that the probe is just detectable when it produces some criterion increase in the response. In other words, the model assumes that the threshold amplitude, A, of a test probe is reached when

$$R(I + A) - R(I) = \delta \qquad (3)$$

where δ is the criterion increase in response. [The predicted values for A are obtained by substituting equation (2) into equation (3) and solving for A.] The curve labeled "no adaptation" in Fig. 1(B) shows the predictions of this simple model for probe–flash curves measured on an intense steady background if there were no adaptation mechanisms ($m = 1$, $s = 0$). The curve labeled M shows the predictions when multiplicative adaptation is added to the model ($m = 0.143$, s = 0). The curve labeled M + S shows the predictions when multiplicative and subtractive adaptation are added to the model ($m = 0.143$, $s = 140$).

As can be seen, multiplicative adaptation improves sensitivity by the greatest amount at high flashed-background intensities, whereas subtractive adaptation only improves sensitivity at lower flashed-background intensities. These different effects of multiplicative and subtractive adaptation show that the magnitude of multiplicative and subtractive adaptation produced by a given steady background can be uniquely estimated from two probe–flash curves, one measured in the dark-adapted eye and one in the presence of a steady background. Psychophysical studies have found that equations (2) and (3) accurately fit the probe–flash curves measured on steady backgrounds (Geisler, 1981; Hayhoe, *et al.*, 1987; Hayhoe, 1990), as well as during long-term dark adaptation (Geisler, 1981). The fits for steady backgrounds typically show strong components of both

multiplicative and subtractive adaptation. The fits for long-term dark adaptation show only multiplicative adaptation, revealing an important difference between background and bleaching adaptation (Geisler, 1981; Hahn & Geisler, 1995).

Steady backgrounds

Amplitude thresholds for detecting simple "broad-band" targets (such as spots or rectangles) against steady backgrounds are adequately described by the generalized Weber's function,

$$A = k(I_b + I_d) \quad (4)$$

where A is the amplitude threshold, I_b is the steady background intensity, k is the Weber fraction, and I_d is the so-called "dark-light" constant. We will refer to a curve which plots amplitude threshold as a function of steady adapting-background intensity as a "background-adaptation curve".

Measurements of probe–flash curves against steady backgrounds of various intensities provide a compelling explanation for why background-adaptation curves follow Weber's law (e.g. see Geisler, 1981, 1983). Specifically, the probe–flash data show (a) that multiplicative adaptation (the value of m) is inversely proportional to the steady background intensity at medium and high background intensities; and (b) that subtractive adaptation (the value of s) is proportional to steady background intensity. The effects of these properties of multiplicative and subtractive adaptation are illustrated in Fig. 1(C). The curve labeled "no adaptation" is the background-adaptation curve (probe threshold as a function of steady-background intensity) that would be obtained if there were no adaptation mechanisms. The curve labeled M shows the background-adaptation curve that would be obtained if multiplicative adaptation were the only adaptation mechanism, and if the multiplicative gain (m) were inversely proportional to background intensity at medium and high background intensities (above 2 log td). The curve labeled M + S shows the background-adaptation curve that would be obtained if there were also subtractive adaptation, and if the magnitude of subtractive adaptation (s) were proportional to background intensity. Multiplicative adaptation produces Weber's law (the slope of 1.0 in log–log coordinates); subtractive adaptation shifts the threshold function to the right (in log–log coordinates), which is equivalent to a decrease the Weber fraction, k, at medium and high background intensities. The curve labeled "no adaptation" and the curve labeled M + S in Fig. 1(C) are typical of actual threshold data measured with flashed and steady backgrounds respectively.

In sum, a model consisting of response compression, multiplicative adaptation, subtractive adaptation, and a simple decision rule can account for thresholds under a wide range of background-adaptation conditions. However, this model has only been tested against data for "broad-band" targets, such as spots and rectangles.

In fact, the model *cannot* account for data obtained with "narrow-band" targets such as sine-wave gratings. Specifically, the model does not predict the changes in the background-adaptation curves that have been observed with changes in target spatial frequency. In agreement with the model, amplitude thresholds for low-frequency gratings on steady backgrounds are described by the generalized Weber function [equation (4)]. However, thresholds for high-frequency gratings are not adequately described by the generalized Weber function; for intermediate background intensities the increment–threshold functions have a slope < 1.0 (Kelly, 1972; Van Nes & Bouman, 1967). Furthermore, the size of the region with slope less than 1.0 systematically increases with target spatial frequency. These variations in the shapes of the background-adaptation curves correspond to the fact that the shape of the contrast-sensitivity function (CSF) changes systematically with steady background intensity (Kelly, 1972; Van Nes & Bouman, 1967).

One possible explanation for the changes in the shapes of the background-adaptation curves is based upon the notion of multiple spatial-frequency channels. There is considerable evidence that different spatial-frequency targets are encoded by separate populations of visual neurons (channels) with different spatial tuning characteristics. Within this framework, variations in the shapes of the background-adaptation curves might be due to variations (across channels) in response nonlinearities, multiplicative adaptation mechanisms, subtractive adaptation mechanisms, or some combination of the three. Another possible explanation is based upon the notion of neural reorganization within the retina (which would affect all channels equally). It is possible that the relative strengths of center and surround mechanisms, or the sizes of center and/or surround mechanisms, may be actively modified by the background-adaptation mechanisms.

In order to examine these possibilities, we measured probe–flash curves on adapting backgrounds of various intensities, for a range of target spatial frequencies. Such measurements allow us to determine whether there are variations (across target spatial frequency) in response nonlinearities, multiplicative adaptation mechanisms, or subtractive adaptation mechanisms. They also provide some evidence concerning the neural reorganization hypothesis.

Another reason for carrying out these experiments was simply to obtain parametric data on spatial pattern detection performance under transient adaptation conditions. Such data may be of practical value in predicting and understanding detection performance under transient lighting conditions, such as those occurring when driving from a dark tunnel into daylight.

METHODS

Subjects

A 30-yr-old male and a 22-yr-old female were the primary subjects in the experiment. Three other subjects were tested on a subset of conditions. All subjects had 20/20 corrected Snellan acuity (or better) and normal color vision, as tested using Dvorine color plates. The

subjects had full knowledge of the purpose of the experiment and were extensively practiced prior to any data collection.

Stimuli

The goal of the present experiments was to measure probe–flash curves for sinusoidal grating targets (probes) against adapting backgrounds of various intensity levels. When using sine-wave-grating targets in spatial vision studies, it is desirable for the targets to be localized in space (in order to minimize the effects of retinal inhomogeneity) and in spatial frequency (in order to isolate spatial-frequency-tuned mechanisms). Full-field sinusoidal gratings provide the best frequency localization, but are not well-localized in space. Simply reducing the size of the grating produces a spatially localized target, but introduces spatial transients (spatial-frequency splatter) at the edges, thus degrading spatial-frequency localization.

A grating target with good localization in both space and spatial frequency is the Gabor pattern, which is the product of a Gaussian and a sine wave (Gabor, 1946). Unfortunately, the Gabor pattern is not well-suited for use as the probe in probe–flash studies because the pattern modulates both above and below the background luminance, as shown in Fig. 3(A). One negative consequence of this modulation is that the Gabor pattern requires a uniform background luminance which may produce some light adaptation, making it difficult to measure probe–flash thresholds in the dark-adapted eye. Another negative consequence is that response compression [e.g. equation (1)] should cause detection of the Gabor pattern to shift from the bright bars to the dark bars as flash luminance is increased, potentially complicating interpretation of the threshold data.

A better probe stimulus is the *increment-Gabor* pattern (Hahn & Geisler, 1995), which is the sum of a Gabor pattern and a simple Gaussian of the same amplitude [Fig. 3(B)]. This pattern is described by the following equation

$$I(x,y) = A \exp\left[-\frac{(x-x_0)^2 + (y-y_0)^2}{2\sigma^2}\right] \times \{1 + \sin(2\pi\mu[(x-x_0)\cos\theta + (y-y_0)\sin\theta])\} \quad (5)$$

where A is the amplitude, σ the SD (spatial spread),* μ the dominant spatial frequency, θ the orientation, and (x_0, y_0) the spatial location. This pattern is referred to as an increment-Gabor pattern because it modulates entirely above the background intensity level, like traditional increment-threshold targets (e.g. spots).†

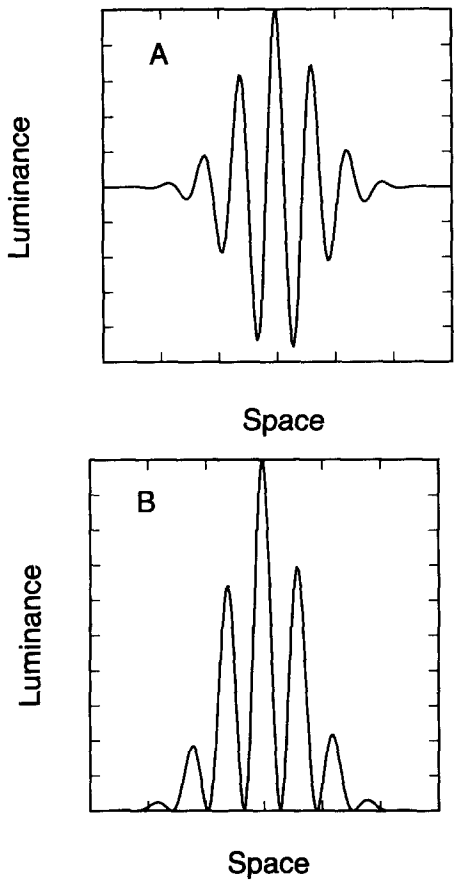

FIGURE 3. Gabor and increment-Gabor test patterns. (A) Intensity profile of a Gabor pattern with an octave bandwidth of 0.5. Notice that the intensity modulates above and below the background. (B) An increment-Gabor of the same bandwidth. The pattern modulates entirely above the background. The test patterns (probes) in the present study were 0.5-octave increment-Gabor patterns. The subject was required to judge whether the pattern was titled 45 deg to the left or 45 deg to the right.

A negative consequence of adding a Gaussian to the Gabor pattern is that the Gaussian contains low-spatial frequency components, which might serve as a basis for detecting the probe. To prevent observers from using the low-frequency components in the Gaussian, we used a detection task in which the observer had to decide whether the increment-Gabor pattern was oriented 45 deg to the left ($\theta = -45$ deg) or 45 deg to the right ($\theta = +45$ deg). The thresholds measured in this task must be based solely upon the frequency content of the Gabor pattern because the frequency components due to the Gaussian are identical for both target orientations. A more complete description of the increment-Gabor pattern can be found in the first paper in this series (Hahn & Geisler, 1995).

Probe–flash curves were measured for increment-Gabor patterns (probes) that were 0.5 octaves in bandwidth, at spatial frequencies of 1, 2, 4, 8, and 12 c/deg. Each probe–flash curve was based on measurements at eight flashed-background intensities ($-\infty$, −0.85, 0.14, 0.91, 1.92, 2.97, 3.56, and 3.98 log td). The entire set of probe–flash curves was measured at four

*The spatial extent (and hence bandwidth) of the target stimulus is determined by the SD parameter of the Gaussian damping function $\sigma = \frac{\sqrt{\ln(c)/2(2^w + 1)}}{\pi\mu(2^w - 1)}$, where μ is the center frequency, w is the octave bandwidth, and c is the criterion height used to define bandwidth. In the present study the bandwidths were 0.5 octaves ($w = 0.5$) at half height ($c = 0.5$).

†Note that it is also possible to measure decrement thresholds using a *decrement-Gabor* pattern created by making the amplitude, A, negative.

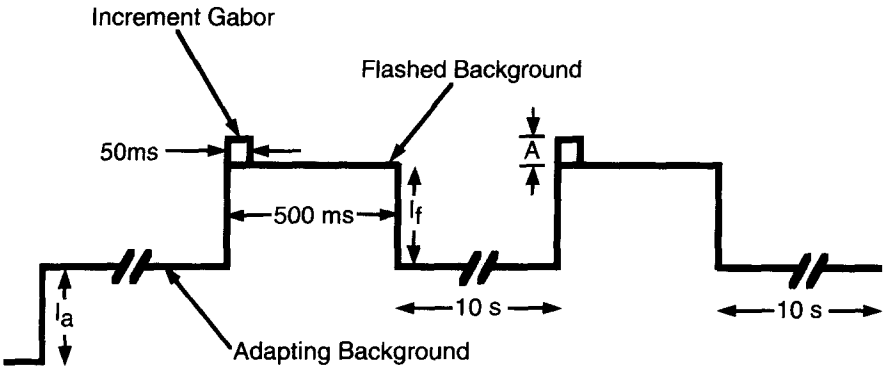

FIGURE 4. Stimulus presentation sequence. Following complete adaptation to the adapting background (intensity = I_a), the increment-Gabor target (spatial frequency = f, amplitude = A) was presented for 50 msec concurrent with the onset of a 500-msec flashed background (intensity = I_f). To insure that the flashed background did not affect the level of light adaptation, 10 sec elapsed between presentations.

levels of steady adapting background ($-\infty$, 1.91, 3.01, and 4.01 log td). Both the flashed background and adapting background were uniform circular fields 6.5 deg in diameter.

Figure 4 shows the stimulus presentation sequence. Following a brief warning tone, the probe was presented for 50 msec concurrent with the onset of a 6.5-deg flashed background, which had a duration of 500 msec. The purpose of the additional 450 msec of the flashed background was to insure that detection of the probe was not occurring in the short-term afterimage (Geisler, 1978; Geisler, 1979). To insure that the subject remained in the appropriate state of adaptation, 10 sec elapsed between stimulus presentations (Geisler, 1979).

Apparatus

The flashed background and steady adapting background were produced in a two-channel Maxwellian view system, as shown in Fig. 5. The increment-Gabor patterns were displayed on a video monitor. The subject and display apparatus were located in a light-sealed room. The subject's head was immobilized by use of a bite bar. The Maxwellian channels and the monitor were viewed through a 3-mm artificial pupil placed directly in front of the eye.

The increment-Gabor stimuli were generated using a PDP 11/73 computer and an ADAGE 3008 graphics processor, and were displayed on an Electrohome monitor, model EDP58XL. This monitor, which has a green (P53) phosphor, and a 1300-line resolution limit, was run at a frame rate of 120 Hz in a non-interlaced mode. The pixel rate was set to produce images 256 × 256 pixels in size. The monitor was adjusted to limit its luminance range to 0–20,000 cd/m^2 (0–100,000 td).

The light source for the two channels of the Maxwellian view system was a Ushio FCR12V-100 W halogen lamp mounted in an Oriel 66182 lamp housing. The presentation of images in the two channels was computer-controlled with an electro-mechanical shutter system which has a transition time of <1 msec. The intensities of the images were controlled by placing Kodak neutral-density filters in the appropriate channel.

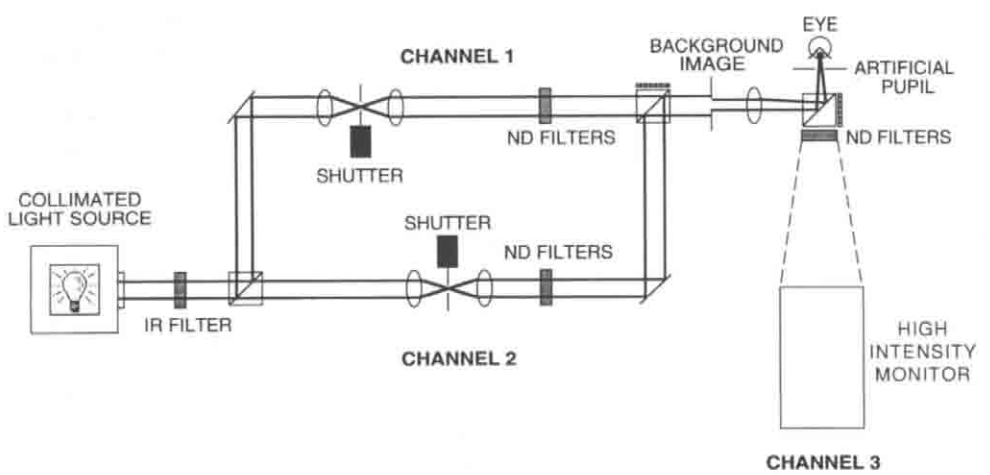

FIGURE 5. The stimuli were presented via a three-channel optical system consisting of a two-channel Maxwellian-view system, in combination with a high-intensity, high-resolution monitor. The monitor was in "normal" (not Maxwellian) view. The outputs of all channels passed through an artificial pupil before entering the eye. Channel 1 was used to deliver the flashed background, Channel 2 the adapting background, and Channel 3 the increment-Gabor targets.

Warning tones and response feedback were provided by a speaker placed near the subject.

Calibration

The basic calibration procedures are described in the companion paper (Hahn & Geisler, 1995). However, several additional precautionary measures were needed to ensure that the high-intensity monitor (which was unique to this study) produced accurate stimuli. First, Kodak neutral density filters were placed between the subject and the monitor in order to keep the monitor operating in its upper luminance range, where single DAC steps produce small log luminance steps. Second, we found that prolonged presentation of full-field patterns produced an upward drift in luminance. Utilizing duty cycles of $< 10\%$ alleviated this problem; the duty cycle for the experiments described here was approx. 0.5%.

Procedure

A complete experimental session consisted of measuring thresholds for a single combination of spatial frequency and steady adapting-background intensity, over the full range of flashed-background intensities. The flashed backgrounds always started at 0.0 td ($-\infty$ log td) and increased toward the maximum. Each threshold was measured three times, in separate sessions.

Prior to the first trial, there was a 10-min period of dark adaptation, followed by 2 min of adaptation to the steady background, which then remained present for the duration of the experimental session. Fixation was provided on the monitor by a pattern of five fixation dots forming an imaginary cross, with one dot in the center. The central fixation dot was extinguished 1 sec before presentation of the probe in order to reduce interference effects.

Because a fixed number of cycles were used for all targets (a fixed 0.5-octave bandwidth), the 1-c/deg target was too large to fall completely inside the rod-free fovea. To isolate cone responses in the dark-adapted condition, thresholds were measured on the cone plateau during a 2-min interval, which occurred 6 min after the offset of a 4.6-log td adapting field.

Most of the thresholds were measured using a method of adjustment; however, a forced-choice staircase method was also used in a subset of conditions as a check on the validity of the adjustment measurements. As will be described below, the two methods gave very similar results.

In the adjustment task, the orientation of the increment-Gabor pattern alternated from trial to trial, and the subject adjusted the amplitude until the two orientations became just indistinguishable. Approximately 1 min elapsed between the completion of a threshold measurement and the presentation of the next flashed-background intensity level.

In the forced-choice task, the orientation of the grating was random from trial to trial, and the subject indicated, after each presentation, whether the grating was oriented to the left or right. The subject's response was immediately followed by feedback indicating whether the response was correct or incorrect. The amplitude of the grating was adjusted in a two-down/one-up staircase procedure (Levitt, 1970); the average of the last six staircase reversals gave an estimate of the 70.7% point on the psychometric function. Each reported threshold was based upon the average of two staircase estimates (12 reversals).

RESULTS

Probe–flash functions for subjects MJM and PTK in the dark-adapted eye are shown in Fig. 6. Each symbol represents the average of three threshold measurements. The average SE (across all the data) is smaller than the diameter of the symbols. As can be seen, there is fairly good agreement between the subjects. In general, for all spatial frequencies, the slopes of the increment–threshold functions increase continuously, reaching values of > 1.5 at 4 log td. When the flashed background is off (left-most data points), the thresholds for the different spatial frequencies are spread out over a range of approx. 1 log unit, with the higher spatial frequencies giving the higher thresholds. The spread of the thresholds decreases

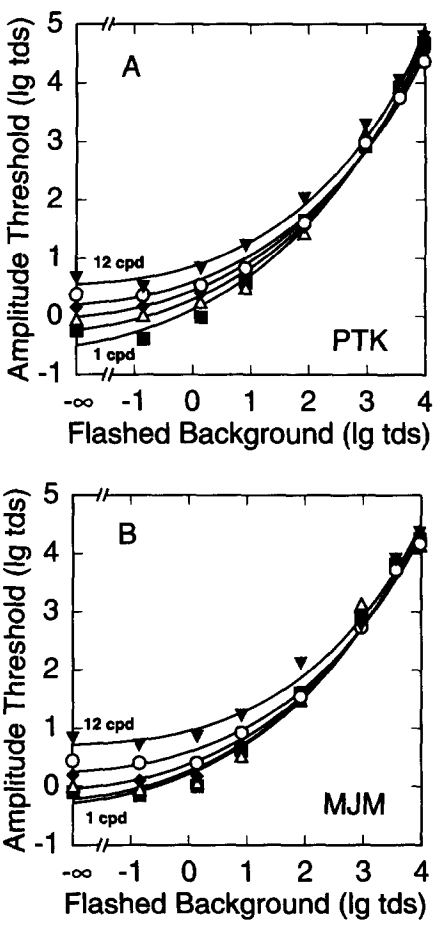

FIGURE 6. Probe–flash curves measured in the dark-adapted eye for increment-Gabor probes at five spatial frequencies: 1 c/deg (■), 2 c/deg (△), 4 c/deg (◆), 8 c/deg (○), 12 c/deg (▼). The symbols represent the average of three measurements. The curves are the best fits of equations (1) and (3). The estimated parameter values of R_{max} and α are given in Fig. 9. See the text for details of the fitting procedure. (A) Subject PTK. (B) Subject MJM. For both subjects the average SEs are smaller than the symbols, and hence are not shown.

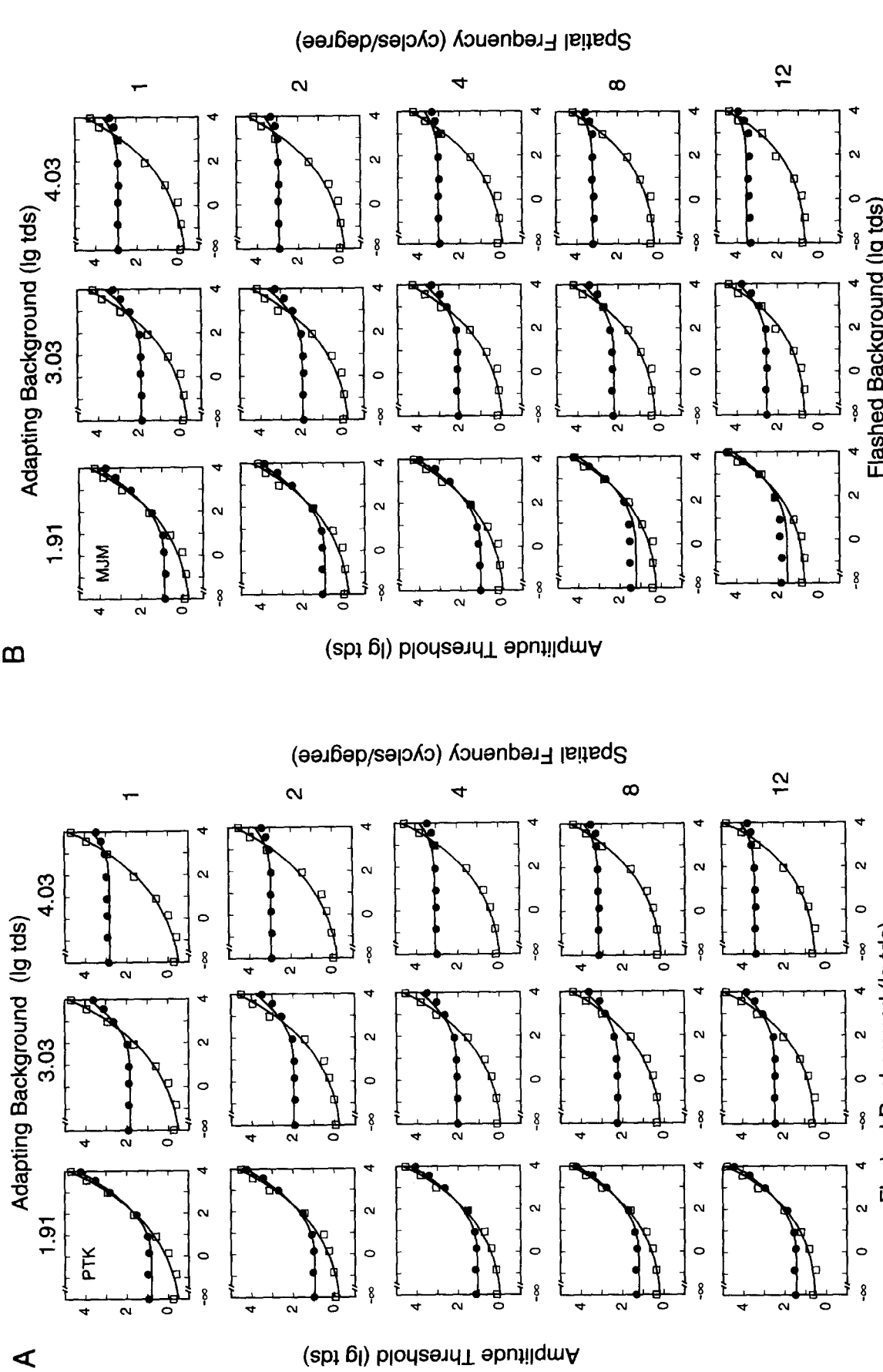

FIGURE 7. Probe–flash curves measured against steady adapting backgrounds. In each plot the circles represent the thresholds obtained for the adapting-background intensity shown at the top of the figure and the probe spatial frequency indicated at the right of the figure. The squares are the data for the dark-adapted eye (from Fig. 6), and are shown for reference. The curves represent the best fits of a simple model, where multiplicative and subtractive adaptation are assumed to be independent of target spatial frequency. The curves through the open squares are the fits obtained with the parameters given in Fig. 9. All of the remaining predictions were obtained with just two free parameters, β and γ, representing the strength of multiplicative and subtractive adaptation as a function of adapting-background intensity [see equations (8) and (9)]. (A) Subject PTK. Parameters: $\beta = 62.9$, $\gamma = 0.89$. (B) Subject MJM. Parameters: $\beta = 55.4$, $\gamma = 0.89$. SEs for both subjects are smaller than the symbols.

substantially as the flashed-background intensity increases.

Data for the three steady adapting background levels are plotted in Fig. 7 as solid circles (the open squares are the thresholds obtained in the dark-adapted eye, and are shown for reference). Again, each symbol represents the average of three threshold measurements obtained in separate sessions. In this figure, the average SEs were 0.049 for MJM and 0.036 for PTK, which are only a fraction of the diameter of the symbols. The data are organized into rows and columns. Each row shows the data for the spatial frequency indicated on the right of the figure; each column shows the data for the adapting background intensity indicated at the top of the figure. As one would expect, the curves tend to flatten with increasing adapting-background intensity. However, within each adapting level, the data exhibit some of the same general trends obtained in the dark-adapted eye; there is a systematic ordering of the thresholds with spatial frequency (higher frequencies have higher thresholds) and the spread of the thresholds decreases as the flashed-background intensity increases.

Figure 8 shows the results of the control experiment, in which data were collected on a subset of the conditions using a two-down/one-up forced-choice staircase method. To avoid the difficulty of measuring forced-choice thresholds on the cone plateau, the control data were measured with an adapting background of 1.91 log td. The open symbols are the thresholds measured with the forced-choice procedure, and the solid symbols [which are the same as the data in Fig. 7(B)] are the thresholds measured with the adjustment procedure. Each open symbol represents the average of 12 staircase reversals. As can be seen, the probe–flash curves obtained with the two methods are very similar; the primary difference is that the thresholds obtained with the forced-choice method are slightly higher. These results extend those of Kelly and Savoie (1973), who found that the adjustment and forced-choice methods yielded similar thresholds for detection of sine-wave gratings on steady adapting backgrounds.

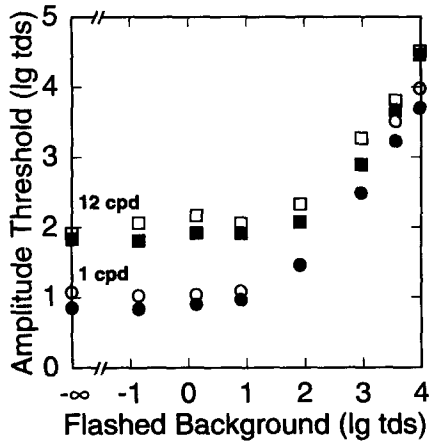

FIGURE 8. Results of a control experiment comparing data collected using a two-down/one-up forced-choice staircase method (□, ○) and the method of adjustment (■, ●), for target spatial frequencies of 1 and 12 c/deg. The adapting-background intensity was 1.91 log td. Except for a slight, but consistent, overall shift in log threshold, the results obtained from the two methods appear to be equivalent.

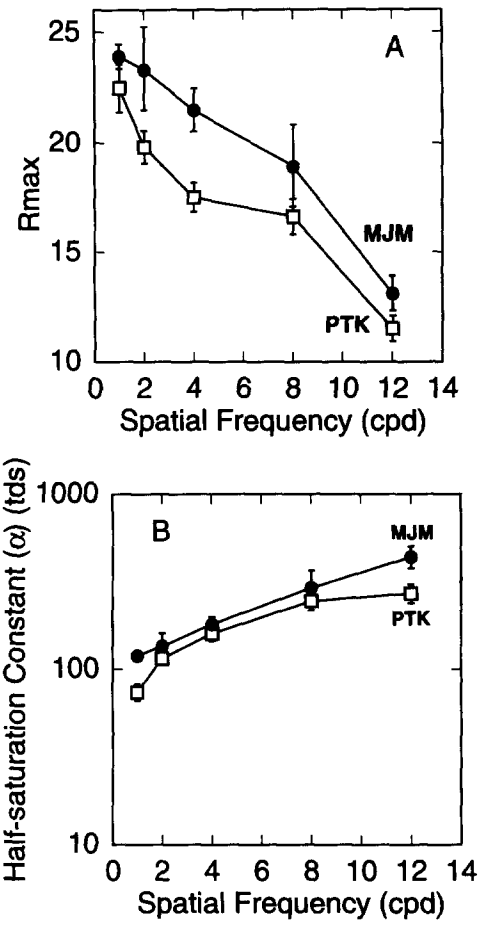

FIGURE 9. (A) R_{max} as a function spatial frequency, in the dark-adapted eye for subjects MJM (●) and PTK (□). (B) Log half-saturation constant, α, as a function of spatial frequency in the dark-adapted eye for subjects MJM (●) and PTK (□). The error bars represent 95% confidence intervals on the parameters. The estimated values of n varied little with spatial frequency and hence are adequately represented by the average for each subject: MJM, $n = 0.55$; PTK, $n = 0.53$.

DATA ANALYSES

The data were analyzed using the theoretical framework (described in the Introduction) that we and others have used in the past to interpret probe–flash data. Specifically, we attempted to fit the data with a model consisting of a compressive non-linearity [equation (1)], combined with multiplicative and subtractive adaptation [equation (2)], and a simple, fixed-criterion decision rule [equation (3)]. The initial questions were: (i) can the model fit data obtained with a range of sine-wave grating targets, and if so, (ii) how do the nonlinearities and adaptation mechanisms vary with target spatial frequency?

Within the model, changes in δ can be exactly mimicked by changes in R_{max}; thus δ can be set to 1.0 without loss of generality. The amplitude thresholds, A, predicted by the model can be solved for explicitly by substituting equation (2) into equation (3):

$$A = \frac{\alpha}{m}\left(\frac{r}{1-r}\right)^{1/n} - I_f - I_b + s \qquad (6)$$

where

$$r = \frac{1 + R(I_f + I_b)}{R_{max}}. \quad (7)$$

The "solver" module of Microsoft Excel 4.0 was used to fit these equations to the threshold data using a minimum squared error criterion (in log units). The fits were confirmed using STEPIT (Chandler, 1969). The 95% confidence intervals on the parameters were computed using the FIDO module in STEPIT.

Analysis 1: spatial-frequency-independent adaptation. The different shapes of the probe–flash curves in the dark-adapted eye (Fig. 6) imply that the response nonlinearity is different for different target spatial frequencies. However, the possibility remains that the magnitudes of multiplicative and subtractive adaptation are invariant with target spatial frequency.

To examine this possibility, we first fit the model to the probe–flash curves measured in the dark-adapted eye, allowing all the parameters of the nonlinear response function (R_{max}, α, n) to vary across spatial frequency. The estimated value of the exponent n varied little with target spatial frequency; in fact, the fits were equally good when n was fixed at the average value for the subject. The best fits (with n fixed at the subject's average) are shown by the curves passing through the open symbols in Fig. 7. Figure 9 shows the estimated values of R_{max} and α as a function of spatial frequency. As can be seen, the peak response, R_{max}, decreases with spatial frequency, and the half-saturation constant, α, increases with spatial frequency. The variations in α could be due to differences in gain across different neural populations; the variations in R_{max} could be due to differences in the peak response of different neural populations, or perhaps to differences in neural pooling within different neural populations.

Earlier studies of the effects of background adaptation on probe–flash curves, measured with spot targets, found that multiplicative gain decreased in inverse proportion to the adapting background intensity at medium to high background intensities (e.g. Geisler, 1981). Although not explicitly stated in Geisler (1981), the multiplicative gain factor was adequately described by the following function (see Fig. 8 in Geisler, 1981):

$$m(I_b) = \frac{\beta}{I_b + \beta} \quad (8)$$

where I_b is the adapting background intensity and β is a constant. (Note that when the eye is dark-adapted, $I_b = 0.0$, then $m = 1.0$.) In that same study, the subtractive factor was found to be an approximately

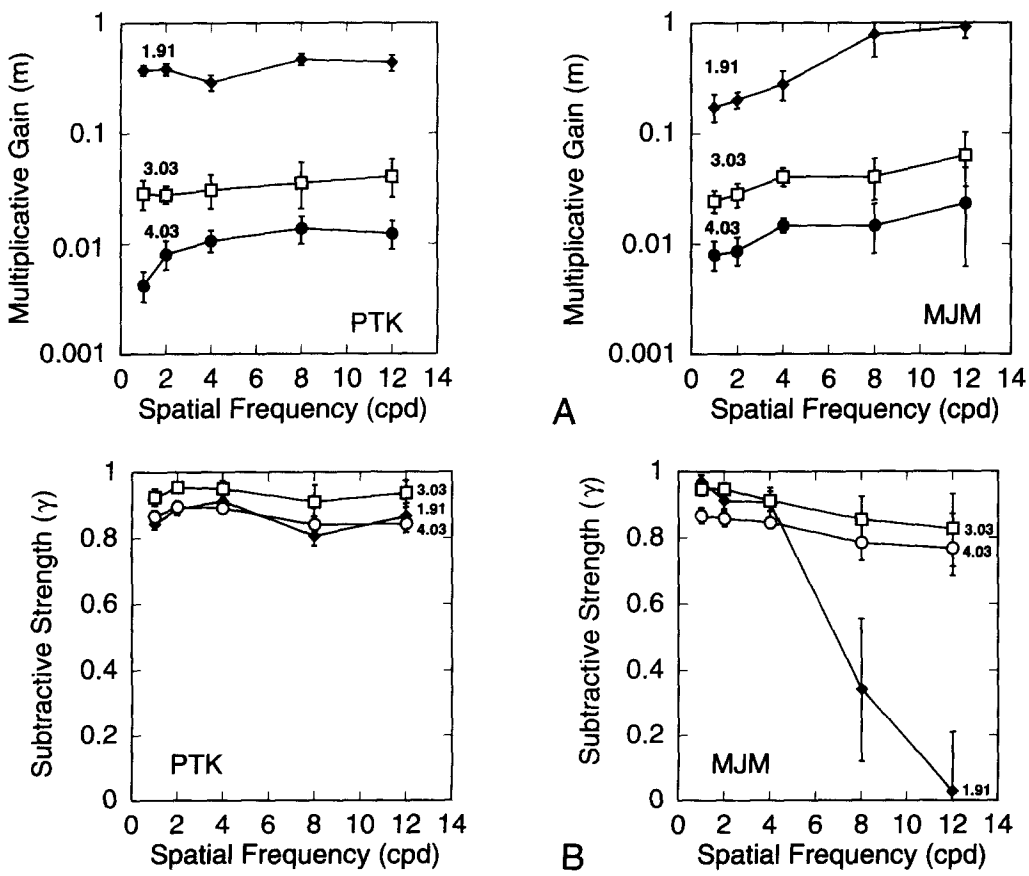

FIGURE 10. (A) Multiplicative gain, m, as a function of spatial frequency, for three adapting-background intensities. Within a given background level, m was relatively invariant with the exception that subject MJM exhibited almost no multiplicative adaptation at a background level of 1.91 log td, for spatial frequencies above 8 c/deg [see Fig. 7(B)]. The error bars represent 95% confidence intervals on m. (B) Subtractive strength, γ, as a function of spatial frequency, for three adapting background levels. For all background levels and spatial frequencies tested, γ was relatively invariant with the exception that subject MJM exhibited almost no subtractive adaptation at a background level of 1.91 log td, for spatial frequencies above 8 c/deg [see Fig. 7(B)]. The error bars represent 95% confidence intervals on γ.

constant proportion of the adapting background intensity,

$$s(I_b) = \gamma I_b \quad (9)$$

where γ is the subtractive strength—the fraction of the adapting background intensity effectively subtracted from the input. (Note that when the eye is dark-adapted, $I_b = 0.0$, then $s = 0.0$.) The curves through the solid circles in Fig. 7 show the fit of the model for $\gamma = 0.894$ (89.4% background subtraction) and $\beta = 62.7$ (PTK) and $\gamma = 0.888$, $\beta = 55.4$ (MJM). Clearly, the model in this form accounts for a large percentage of the variance in the data.

Analysis 2: spatial-frequency-dependent adaptation. The reasonably good fits of the above model suggest that the strengths of multiplicative and subtractive adaptation are largely independent of target spatial frequency. However, subject MJM did systematically violate this rule when the background-adaptation intensity was 1.91 log td. Specifically, the probe–flash curves for the low spatial-frequency targets (1, 2, and 4 c/deg) display evidence of multiplicative and subtractive adaptation, whereas those for the high spatial-frequency targets (8 and 12 c/deg) show little evidence of either multiplicative or subtractive adaptation. Notice, for example, that for the low-frequency targets the probe–flash curves cross at high flashed-background intensities, whereas they do not cross for the high-frequency targets. To quantify these spatial-frequency-dependent changes in adaptation, we fit the model to all the data allowing the parameters β and γ to vary with spatial frequency and adapting background intensity. Figure 10 shows the estimated values of m [see equation (8)] and γ, for both subjects MJM and PTK. As can be seen, the estimated parameters are roughly constant with spatial frequency, except for subject MJM when the background intensity is 1.91 log td. Allowing β and γ to vary with spatial frequency improves the fit to MJM's data at 8 and 12 c/deg (when the background is 1.91 log td), but otherwise the fits differ very little from those in Fig. 7.

The large difference in estimated adaptation parameters at 1.91 log td for the two subjects prompted us to test several other subjects at this background level, and in the dark-adapted eye. Figure 11 shows the estimated values of m and γ when they were allowed to vary with spatial frequency. As with subject PTK, there was relatively little change in the adaptation parameters with spatial frequency, suggesting that subject MJM's pattern of results is less common.

Exponents of the response nonlinearities

In the original form of the Michaelis–Menten equation used by Naka and Rushton (1966), the value of the exponent, n, was implicitly set at 1.0. Later, Boynton and Whitten (1970) found that their late-receptor-potential data were best fit with an exponent of 0.7. This value has also been obtained in psychophysical studies (Geisler, 1979; Hayhoe *et al.*, 1992), although some studies have found a value closer to 1.0 (Hayhoe *et al.*, 1987). In the current study, the best fits were obtained

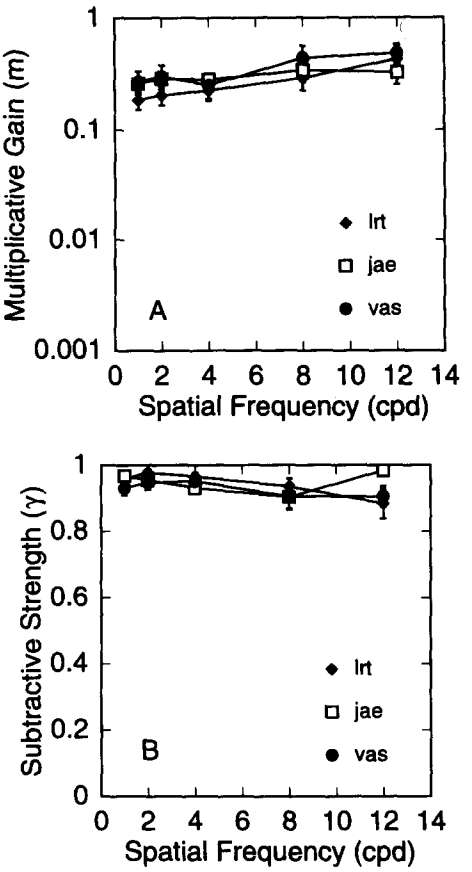

FIGURE 11. (A) Multiplicative gain, m, for three additional subjects at a background of 1.91 log td. (B) Subtractive strength, γ, for three additional subjects at a background of 1.91 log td. The error bars represent 95% confidence intervals on the parameters. Both m and γ were relatively invariant; hence these additional subjects are more similar to subject PTK than subject MJM.

with an exponent of approximately 0.5, a value smaller than reported previously.

There are several factors that may have contributed to this apparent discrepancy, but probably the most important is the range of flashed-background intensities included in the fitting procedure. In the present study, and in earlier work from this laboratory, the estimate of the exponent was obtained by fitting thresholds measured over a wide range of flashed-background intensities: from the dark up to 4 log td or greater. In the studies of Hayhoe, Hood *et al.*, the exponent was usually estimated by fitting the thresholds obtained over a more restricted range of flashed-background intensities: from the dark up to 3 log td or less. When the thresholds for flashed backgrounds above 3 log td (in the present study) are excluded from the fitting procedure, the exponent (n) increases to approx. 0.68. Table 1 shows the estimates of n, for four different studies, when the fits were restricted to flashed backgrounds below 3.0 log td and to flashed backgrounds below 4.0 log td. As can be seen, restricting the data to lower flashed-background levels causes an increase in the exponent n. More important, the table shows that when the various studies are fitted using the same data range (and fitting procedure), the estimates of the exponents agree reasonably well; in other words, the data are in good agreement across studies. Therefore, the

TABLE 1. Values of the exponent n, for several studies, estimated using the fitting procedure described in this paper

Study	≤ 3 log td	≤ 4 log td
Hayhoe, Levin, and Koshel (subject MEL)	0.69	0.51
Hayhoe, Levin, and Koshel (subject RJK)	0.69	0.57
Geisler (1981) (subject WSG)	0.73	0.67
Geisler (1975) (subject WSG)	0.73	0.63
Kortum and Geisler (subject PTK)	0.61	0.53
Kortum and Geisler (subject MJM)	0.69	0.50
Kortum and Geisler (subject VAS)	0.73	0.53

The column labeled "≤ 3 log td" lists the values of n obtained when the fit was restricted to background flash intensities below 3 log td. Similarly, the column labeled "≤ 4 log td" lists the values n obtained when the fit included background flash intensities up to 4 log td. The estimate of n increases when the data range is decreased, but, more important, the data from the various studies yield similar estimates of n.

lower values of n obtained in the present study are not indicative of any fundamental differences between grating and spot targets, but rather, reflect differences in the range over which the data were fitted.

Which procedure for estimating the exponent is better? Parsimony would suggest using as much of the available data as possible. However, one argument for not including the data at high flashed-background intensities is the possibility that detection might be occurring in a short-term afterimage (Geisler, 1978; Hayhoe *et al.*, 1992). Geisler (1978) found that above 4 log td, detection was possible in the short-term afterimage seen following background offset (with a 500-msec flashed background). This result would suggest including all data up to 4 log td. Another possibility is that detection might be occurring in a negative afterimage seen against the flashed background (Adelson, 1982). Detection of a negative afterimage might occur at lower flashed-background intensities (Hayhoe *et al.*, 1992). If so, it would be better to include only those thresholds measured at very low flashed-background intensities.

If negative afterimages were mediating thresholds in the range of 3–4 log td in our experiments, then at threshold (or slightly above threshold), the increment-Gabor targets should have appeared in reversed phase. To test this possibility, we had (two) subjects judge the phase of 1-c/deg increment-Gabor targets on flashed backgrounds of 3.5 and 4.0 log td. On each trial the phase was shifted by 180 deg and the subject judged to which side of the screen's center the brighter stripe appeared. The results clearly indicated that there was no phase reversal, and hence, that detection was not occurring in a negative afterimage. We conclude that it is appropriate to use the entire range of data in estimating the exponent of the response nonlinearity.

However, it is important to note that these details of the fitting procedure are not very relevant to many of the major aims of the present study (or to those of most earlier studies), which were to characterize the subtractive and multiplicative adaptation mechanisms. As long as good fits are obtained (which was the case), the measurements of the subtractive and multiplicative adaptation effects are unaffected. We also note that although the fitting procedure affects the estimated exponent, it does not affect our finding that the exponent is essentially constant with target spatial frequency, or that the response nonlinearities vary systematically with target spatial frequency.

DISCUSSION

A major goal of this study was to obtain parametric data on spatial-pattern detection performance under transient adaptation conditions. To do this we measured probe–flash curves for sinusoidal targets (increment-Gabor targets) that were localized in space and spatial frequency. Probe–flash curves were measured for a wide range of target spatial frequencies and for a wide range of background-adaptation intensities (ambient light levels). The probe–flash curves were found to vary in shape with target spatial frequency. This change in shape was qualitatively similar for all background-adaptation intensities. At low flashed-background intensities the probe–flash curves were highly separated as a function of spatial frequency, the higher the spatial frequency the higher the threshold. However, as flashed-background intensity increased, the separation of the probe–flash curves decreased substantially. For example, in the dark-adapted eye the probe–flash curves became nearly superimposed above 2 log td.

The change in the shape of the probe–flash curves with target spatial frequency suggests that the background flash is simultaneously driving more than one nonlinear response function and that these different nonlinear response functions are associated with neural channels tuned to different ranges of spatial frequency or size. An alternative, but *a priori* unlikely, explanation is that the flashed background activates an essentially instantaneous adaptation mechanism that alters spatial-frequency tuning within a single neural channel based upon flashed-background intensity. We cannot refute this alternative on the basis of the available psychophysical data; however the physiological data certainly suggest that there are at least two channels in the retina (the populations of so-called M and P neurons) which have different nonlinear response functions (Kaplan & Shapley, 1982; Derrington & Lennie, 1984; Shapley & Perry, 1986). For the purpose of the present discussion we adopt the first, more plausible, framework.

Site of adaptation

The probe–flash curves measured for different adapting-background intensities indicate that the strengths of multiplicative and subtractive adaptation are relatively constant across target spatial frequency. This result would seem to suggest that the site of adaptation is prior to the separation of information into the retinal spatial channels (e.g. prior to the M and P pathways). Given that the separate retinal spatial channels apparently begin at the level of the bipolar cells (e.g. see Sterling, 1990; Wässle & Boycott, 1991) this would place the adaptation in the photoreceptor or in the

receptor–bipolar synapse [although receptor adaptation does not appear to be strong enough by itself to account for the psychophysical effects (e.g. see Schnapf *et al.*, 1990; Schnapf, Schneeweis & Kraft, 1994; Hood & Birch, 1993)].

An alternative possibility is that some components of the subtractive and multiplicative adaptation mechanisms operate within the retinal spatial channels (e.g. in the bipolar cells). This hypothesis gains some support from the fact that the magnitudes of subtractive and multiplicative adaptation demonstrate small, but systematic, decreases as spatial frequency increases; these effects are most pronounced in the data from subject MJM. MJM shows little subtractive or multiplicative adaptation at low background levels in the high spatial frequency range, but shows substantial adaptation in the low spatial frequency range (see Fig. 10). This could not happen if the adaptation mechanisms were operating entirely within the photoreceptors.

MJM's pattern of results (and the smaller effects observed for the other subjects) may be consistent with known retinal physiology. If those neurons most sensitive to high spatial frequencies (presumably the P-cells) have lower gain [as suggested by primate ganglion-cell physiology (e.g. Derrington & Lennie, 1984; Shapley & Perry, 1986)], and if the adaptation mechanisms do not engage until the background is intense enough to drive the neurons to near or above half-saturation [as suggested by vertebrate retinal physiology (e.g. see Shapley & Enroth-Cugell, 1984)], then one would expect to observe decreases in adaptation strength as spatial frequency increases (especially when the background intensity is low).

Noise and spatial mechanisms

One criticism that could be leveled against our theoretical analyses is the simplicity of the theoretical framework. The two most obviously questionable assumptions are (i) that threshold is reached when the difference in neural responses reaches some fixed criterion amount [equation (3)], and (ii) that the neural response to a two-dimensional retinal pattern can be represented by a simple one-dimensional function [equation (1)].

In any real system, discrimination performance is limited by the noisiness of the internal responses and decision mechanisms. The assumption that a fixed difference in response is required for threshold is equivalent to assuming a constant level of response or decision noise, independent of the average response level. However, physiological evidence clearly indicates that the variance of neural response in the cortex grows approximately in proportion to the mean response (Snowden, Treue & Andersen, 1992; Tolhurst, Movshon & Dean, 1983; Vogels, Spileers & Orban, 1989), independent of the stimulus conditions that produced that mean response (Geisler & Albrecht, 1995; Vogels *et al.*, 1989). Thus, inclusion of neural noise of this form would certainly make the theoretical analyses more plausible. To check on the importance of the particular neural noise assumption, all the data were re-analyzed assuming that the variance of the neural noise is proportional to the mean response. Although the estimated parameters of the nonlinearities were changed somewhat, there was no change in the goodness-of-fit, nor in the conclusions reached concerning multiplicative and subtractive adaptation and their relationship to target spatial frequency.

Another source of noise which our analysis does not address directly is photon noise. Photon noise is similar to cortical neural noise in that the variance in the number of photons absorbed in a fixed time period is proportional to the mean number absorbed in that same time period. Photon noise is probably not a major limiting factor in photopic sensitivity (Geisler, 1989; Graham & Hood, 1992a). Nonetheless, whatever the contribution of photon noise, it must be reflected in response variance properties of cortical neurons (i.e. variance proportional to the mean), which, as mentioned above, we have already considered.

Although we have used a simple one-dimensional model to interpret the data, we have also implemented a more elaborate two-dimensional spatial model (which will be presented in a subsequent paper). The two-dimensional version leads to the same conclusions concerning multiplicative and subtractive adaptation and their relationship to target spatial frequency. Recently Graham and Hood (1992b) developed a two-dimensional (space–time) model in much the same spirit as the present model, but with an emphasis on temporal dynamics and temporal data. Their model is able to predict the effects of light adaptation on temporal contrast sensitivity and on flashed-background increment–thresholds. Although one cannot be certain, it is possible that a complete three-dimensional model (representing a merging of these space–space and space–time models) would lead to conclusions concerning multiplicative and subtractive adaptation, similar to those arrived at with the simple analysis presented here.

Descriptive model

Although there are some individual differences in the results of the present experiments, and there are some alternative models that might account for the general pattern of results (which will be described in a subsequent paper), it is possible to summarize the entire set of data with a simple descriptive model that may be of some practical value in predicting target detectability under different transient and steady-state adaptation conditions. This descriptive model represents the performance of an "average" observer. The equations that describe this average observer are as follows:

$$A = \frac{\alpha}{52.5/(I_b + 52.5)}\left(\frac{r}{1-r}\right)^{1/n} - I_f - 0.1I_b \quad (10)$$

$$r = \frac{1 + R(I_f + I_b)}{R_{max}} \quad (11)$$

$$R(I_f + I_b) = \frac{R_{max}(I_f + 0.1I_b)^n}{(I_f + 0.1I_b)^n + \left(\frac{I_b + 52.5}{52.5}\alpha\right)^n} \quad (12)$$

$$R_{max} = -0.9\mu + 23.7 \quad (13)$$

$$\alpha = 22.63\mu + 77.27. \quad (14)$$

In determining the parameter values used in this equation, we first computed the geometric mean (across subjects) of R_{max}, α, and n, for each spatial frequency. Using these geometric means, optimum values of β and γ were determined by simultaneously fitting all 30 experimental data conditions (15 per subject) to minimize the squared error. Finally, fitting a straight line through the geometric means of R_{max} and α allows us to replace them with the frequency dependent equations (13) and (14), where μ is the spatial frequency of interest.

Explanation of Weber's law and the square-root law

The data and analyses described here suggest simple explanations for Weber's law and the square-root (deVries–Rose) law. For all spatial frequencies tested, we found that multiplicative gain was inversely proportional to adapting-background intensity, in the range of medium-to-high background intensities. These results confirm and extend earlier work with broad-band (spot) targets and strongly support the hypothesis that Weber's law is the consequence of multiplicative adaptation mechanisms. Without these mechanisms, detection threshold would follow a continuously accelerating function, saturating at high background intensities. For all spatial frequencies tested, subtractive adaptation was found to be proportional to adapting-background intensity; thus, subtractive adaptation apparently does not contribute to the production of Weber's law, although it does improve overall sensitivity (i.e. it produces decreases in the Weber fraction).

The probe–flash curves obtained in the dark-adapted eye, and in all other fixed-adaptation conditions, were found to systematically change with target spatial frequency. These results suggest that different spatial frequencies are being detected by different spatial mechanisms (channels), which have different nonlinear response functions. This hypothesis gains support from the fact that all the data could be fit by combining simple multiplicative and subtractive adaptation mechanisms with the nonlinearities estimated from the probe–flash curves measured in the dark-adapted eye. Another hypothesis is that the different spatial channels have different noise characteristics. However, this seems less likely given that the simple noise characteristics of monkey and cat cortical cells do not seem to vary with stimulus spatial frequency (e.g. Geisler & Albrecht, 1995). Thus, we are led to conclude that the most likely explanation for the systematic changes in background-adaptation curves with target spatial frequency (i.e. the increased square-root regions with increasing target spatial frequency) is spatial channels with different nonlinear response functions.

REFERENCES

Adelson, E. H. (1982). The delayed rod afterimage. *Vision Research, 22*, 1313–1328.

Alpern, M., Rushton, W. A. H. & Torii, S. (1970). Signals from cones. *Journal of Physiology, 207*, 463–475.

Boynton, R. M. & Whitten, D. N. (1970). Visual adaptation in monkey cones: Recordings of late receptor potentials. *Science, 170*, 1423–1426.

Chandler, J. P. (1969). STEPIT—Finds local minima of a smooth function of several parameters. *Behavioral Science, 14*, 81–82.

Craik, K. J. W. (1940). The effect of adaptation on subjective brightness. *Proceedings of the Royal Society of London B, 128*, 232–247.

Derrington, A. M. & Lennie, P. (1984). Spatial and temporal contrast sensitivities of neurones in lateral geniculate nucleus of macaque. *Journal of Physiology, London, 357*, 219–240.

Gabor, D. (1946). Theory of communication. *Journal of the Institute of Electrical Engineers (London), 93*, 429–457.

Geisler, W. S. (1978). Adaptation, afterimages and cone saturation. *Vision Research, 18*, 279–289.

Geisler, W. S. (1979). Initial-image and afterimage discrimination in the human rod and cone systems. *Journal of Physiology, London, 294*, 165–179.

Geisler, W. S. (1981). Effects of bleaching and backgrounds on the flash response of the visual system. *Journal of Physiology, London, 312*, 413–434.

Geisler, W. S. (1983). Mechanisms of visual sensitivity: Backgrounds and early dark adaptation. *Vision Research, 23*, 1423–1432.

Geisler, W. S. (1989). Sequential ideal-observer analysis of visual discriminations. *Psychological Review, 96*, 267–314.

Geisler, W. S. & Albrecht, D. G. (1995). Bayesian analysis of identification performed in monkey visual cortex: Nonlinear mechanisms and stimulus certainty. *Vision Research*. In press.

Graham, N. & Hood, D. C. (1992a). Quantal noise and decision rules in dynamic models of light adaptation. *Vision Research, 32*, 779–787.

Graham, N. & Hood D. C. (1992b). Modeling the dynamics of light adaptation: The merging of two traditions. *Vision Research, 32*, 1373–1393.

Hahn, L. W. & Geisler, W. S. (1995). Adaptation mechanisms in spatial vision—I. Bleaches and backgrounds. *Vision Research, 35*, 1585–1594.

Hayhoe, M. M. (1990). Spatial interactions and models of adaptation. *Vision Research, 30*, 957–965.

Hayhoe, M. M., Benimoff, N. E. & Hood, D. C. (1987). The time–course of multiplicative and subtractive adaptation process. *Vision Research, 27*, 1981–1996.

Hayhoe, M. M., Levin, M. E. & Koshel, R. J. (1992). Subtractive processes in light adaptation. *Vision Research, 32*, 323–333.

Hood, D. C. (1978). Psychophysical and physiological tests of physiological explanations of light adaptation. In Armington, J., Krauskopf, J. & Wooten, B. (Eds), *Visual psychophysics: Its physiological basis*. New York: Academic Press.

Hood, D. C. & Birch, D. G. (1993). Human cone receptor activity: The leading edge of the a-wave and models of receptor activity. *Visual Neuroscience, 10*, 857–871.

Hood, D. C. & Finkelstein, M. A. (1986). Sensitivity to light. In Boff, K. R., Kaufman, L. & Thomas, J. P. (Eds), *Handbook of perception and human performance* New York: Wiley.

Hood, D. C., Ilves, T., Mauer, E., Wandell, B. & Buckingham, E. (1978). Human cone saturation as a function of ambient intensity: A test of models of shifts in the dynamic range. *Vision Research, 19*, 983–993.

Jacobs, G. H. (1965). Effects of adaptation on the lateral geniculate response to light increment and decrement. *Journal of the Optical Society of America, 55*, 1535–1540.

Kaplan, E. & Shapley, R. M. (1982). X and Y cells in the lateral geniculate nucleus of macaque monkey. *Journal of Physiology, London, 330*, 125–143.

Kelly, D. H. (1972). Adaptation effects on spatio-temporal sine-wave thresholds. *Vision Research, 12*, 89–101.

Kelly, D. H. & Savoie, R. E. (1973). A study of sine-wave contrast sensitivity by two psychophysical methods. *Perception & Psychophysics, 14*, 313.

Kleinschmidt, J. & Dowling, J. E. (1975). Intracellular recordings from gecko photoreceptors during light and dark adaptations. *Journal of General Physiology*, *66*, 617–648.

Levitt, H. (1970). Transformed up–down methods in psychoacoustics. *Journal of Acoustical Society of America*, *49*, 467–477.

Naka K.-I. & Rushton, W. A. H. (1966). S-potentials from luminosity units in the retina of fish (*Cyprinicae*). *Journal of Physiology*, *London*, *185*, 587–599.

Normann, R. A. & Werblin, F. S. (1974). Control of retinal sensitivity I. Light and dark adaptation of vertebrate rods and cones. *Journal of General Physiology*, *63*, 37–61.

Sakmann, B. & Creutzfeldt, O. D. (1969). Scotopic and mesopic light adaptation in the cat's retina. *Pflugers Archiv*, *313*, 168–185.

Schnapf, J. L., Schneeweis, D. M. & Kraft, T. W. (1994). Phototransduction in primate photoreceptors. *Investigative Ophthalmology and Visual Science*, *35*, 2001.

Schnapf, J. L., Nunn, B. J., Meister, M. & Baylor, D. A. (1990). Visual transduction in cones of the monkey *Macaca Fascicularis*. *Journal of Physiology*, *London*, *427*, 681–713.

Shapley, R. M. & Enroth-Cugell, C. (1984) Visual adaptation and retinal gain controls. *Progress in Retinal Research*, *3*, 263–346.

Shapley, R. M. & Perry, H. V. (1986). Cat and monkey retinal ganglion cells and their visual functional roles. *Trends in Neuroscience*, *9*, 229–235.

Shevell, S. K. (1977). Saturation in human cones. *Vision Research*, *17*, 427–434.

Shevell, S. K. (1978). The dual role of chromatic backgrounds in color perception. *Vision Research*, *18*, 1649–1661.

Snowden, R. J., Treue, S. & Andersen, R. A. (1992). The response of neurons in areas V1 and MT of the alert rhesus monkey to moving random dot patterns. *Experimental Brain Research*, *88*, 389–400.

Sterling, P. (1990). Retina. In Sherpard, G. M. (Eds), *The synaptic organization of the brain* (pp. 170–213). New York: Oxford University Press.

Tolhurst, D. J., Movshon, J. A. & Dean, A. F. (1983). The statistical reliability of signals in single neurons in the cat and monkey visual cortex. *Vision Research*, *23*, 775–785.

Valeton, J. M. & van Norren, D. (1982). Light-adaptation of primate cones: An analysis based on extracellular data. *Vision Research*, *23*, 1539–1547.

Van Nes, F. L. & Bouman, M. A. (1967). Spatial modulation transfer in the human eye. *Journal of the Optical Society of America*, *57*, 401–406.

Virsu, V. & Lee, B. B. (1983). Light adaptation in cells of macaque lateral geniculate nucleus and its relation to human light adaptation. *Journal of Neurophysiology*, *50*, 864–878.

Vogels, R., Spileers, W. & Orban, G. A. (1989). The response variability of striate cortical neurons in the behaving monkey. *Experimental Brain Research*, *77*, 432–436.

Von Kries, J. (1970). Influence of adaptation on the effects produced by luminous stimuli. In MacAdam, D. L. (Eds), *Sources of color science* Cambridge, Mass.: MIT Press.

Walraven, J., Enroth-Cugell, C., Hood, D. C., MacLeod, D. I. A. & Schnapf, J. L. (1990). The control of visual sensitivity: Receptoral and postreceptoral processes. In Spillman, L. & Werner, J. S. (Eds), *Visual perception: The neurophysiological foundations*. San Diego, Calif.: Academic Press.

Wässle, H. & Boycott, B. B. (1991). Functional architecture of the mammalian retina. *Physiological Reviews*, *71*, 447–480.

Acknowledgements—This research was supported by NIH grant EY02688 and AFOSR grant F49620-93-1-0307 to WSG.